Chalcogenide Letters Vol. 19, No. 9, September 2022, p. 599 - 609

Effect of pre-annealing of Mo foil substrate on CZTSSe thin films and $Mo(S,Se)_2$ interface layer

X. S. Wu[b], J. X. Xu[a,b,*]
[a]*School of Integrated Circuits, Guangdong University of Technology, Guangzhou 510006, China*
[b]*School of Materials and Energy, Guangdong University of Technology, Guangzhou 510006, China*

$Cu_2ZnSn(S,Se)_4$ (CZTSSe) thin film deposited on flexible Mo foil substrate has advantage of high mass specific power and good ductility. However, a thick $Mo(S,Se)_2$ interface layer is easily to be formed between CZTSSe and Mo foil substrate. The ohmic contact property of CZTSSe/Mo is deteriorated by the formation of $Mo(S,Se)_2$. In this work, the Mo foil substrate was pre-annealed to inhibit the growth of $Mo(S,Se)_2$ interface layer. CZTSSe thin films were prepared on the pre-annealed Mo foil substrate by sol-gel and selenization methods. The pre-annealing treatment of Mo foil substrate leads to the oxidation of Mo. During the high temperature selenization process, the MoO_x acts as a buffer layer to suppress the formation of the $Mo(S,Se)_2$ interface layer. With the increase of the pre-annealing temperature of the Mo foil substrate, the thickness of the $Mo(S,Se)_2$ interface layer decreases, and the resistance of CZTSSe/$Mo(S,Se)_2$/Mo structure decreases. The ohmic contact properties of CZTSSe/Mo can be improved by the pre-annealing treatment of metal Mo foil substrates.

(Received June 1, 2022; Accepted September 12, 2022)

Keywords: CZTSSe, Pre-annealing, MoO_x, $Mo(S,Se)_2$, Interface layer

1. Introduction

Semiconducting $Cu_2ZnSn(S,Se)_4$ (CZTSSe) with a kesterite structure has broad prospects in the application of solar cell absorber [1,2]. As a direct band gap p-type semiconductor material, CZTSSe has high absorption coefficients of 10^4 cm^{-1}. Its band gap can be adjusted to a suitable range of 1.0 eV~1.5 eV by the ratio of S and Se. [3–5]. Only a CZTSSe thickness of about 1 to 2 μm is needed to absorb enough incident sunlight [6]. At present, the highest efficiency of the CZTSSe thin film solar cell is 12.7% [7], which still has a huge gap with the theoretical efficiency of 32.2 % [8].

Most reported CZTSSe thin film solar cells use Mo-coated glass as substrates [9–12]. During the high-temperature heat treatment, a $Mo(S,Se)_2$ interface layer can be formed between the CZTSSe absorber layer and Mo back electrode by the sulfurization and selenization reactions of Mo [13–15]. The $Mo(S,Se)_2$ layer leads to the increase of series resistance (R_S) of solar cell,

*Corresponding author: xujiaxiong@gdut.edu.cn
https://doi.org/10.15251/CL.2022.199.599

resulting in a decrease in the conversion efficiency of solar cell [16]. In order to reduce the thickness of $Mo(S,Se)_2$ interface layer, a buffer layer, such as $CuAlO_2$, WSe_2, or VSe_2, can be introduced between CZTSSe and Mo [17–19]. The buffer layer helps to prevent the diffusion of Se atoms to Mo layer, thereby reducing the thickness of $Mo(S,Se)_2$ interfacial layer.

In addition to rigid soda-lime glass substrate, using flexible substrate can expand the application field of CZTSSe solar cells [20–22]. The flexible Mo foil has a compatible thermal expansion coefficient of 5.2×10^{-6} K^{-1}, which is a suitable flexible substrate for CZTSSe solar cell. The structure of flexible CZTSSe thin-film solar cell on Mo foil substrate is Ag/ZnO:Al/i-ZnO/CdS/CZTSSe/Mo. The interface between CZTSSe and Mo foil is also a key factor affecting the performance of CZTSSe solar cell. In our previous work, a $Mo(S,Se)_2$ interface layer with a thickness of about 3 μm can be formed during the fabrication of CZTSSe thin film on Mo foil substrate [23]. Mo foil is more conducive to the formation of $Mo(S,Se)_2$ interface layer than Mo thin film on soda-lime glass substrate. Therefore, it is more essential to adjust the $Mo(S,Se)_2$ interface layer when flexible Mo is used as the substrate of CZTSSe thin film. However, there are few literatures about the interface regulation of CZTSSe/$Mo(S,Se)_2$/Mo foil structure.

As the method of insertion of a buffer layer has been proved to be a useful way to control the growth of $Mo(S,Se)_2$ layer when using Mo-coated glass substrates [18–21], this work proposes a method of pre-annealing of Mo foil substrate before the deposition of CZTSSe. The pre-annealing of Mo foil is expected to lead to the surface oxidation of Mo foil. The metal oxide on the surface of Mo foil can inhibit the sulfurization and selenization reactions of Mo foil during the fabrication of CZTSSe. Compared with the traditional buffer layer method, the pre-annealing of substrate is more facile and convenient as it does not need complex equipment to deposit the buffer layer, such as magnetron sputtering, vacuum evaporation, and plasma enhanced chemical vapor deposition. In this work, the effects of pre-annealing temperature of Mo foil substrate on the phase structures and morphologies of substrate, and the phase structures, morphologies, and electrical properties of CZTSSe samples were studied.

2. Experimental

Flexible metal Mo foil (1.5 cm × 1.5 cm × 0.05 mm) was used as substrate. First, the Mo foil was cleaned successively in deionized water, acetone, anhydrous ethanol, and deionized water by ultrasonics technique. Second, the clean Mo substrate was placed in a tube furnace and pre-annealed in air under standard atmospheric pressure. The substrate was heated with a ramp-up rate of 10 min/°C. The Mo foil substrate was pre-annealed at target temperautres of 300 °C, 400 °C, or 500 °C for 30 min.

Sol-gel method was utilized to deposit CZTSSe thin films. 3.6692 g $Cu(CH_3COO)_2\cdot H_2O$, 2.5385 g $Zn(CH_3COO)_2\cdot 2H_2O$, and 2.2693 g $SnCl_2\cdot 2H_2O$ were dissolved in 8 ml $(C_2H_2OH)_2$, and stirred for 30 min to obtain solution A. Then, 5.5958 g CH_4N_2S was dissolved in a mixed solvent of 10 ml $(C_2H_2OH)_2$ and 2 ml $C_5H_8O_2$, and stirred for 30 min to obtain solution B. Then, the solution A and solution B were mixed and stirred at 60 °C for 60 min to obtain a clear yellow precursor solution. Using a spin coater (Science EZ4, Leibo), the precursor solution was spin-coated on Mo foil substrates with and without pre-annealing first at a low speed of 800 r/min for 20 s and then at a high speed of 3000 r/min for 40 s. After spin coating, the samples were dried

in air at 250 °C for 90 s by drying machinery. The spin-coating and drying steps were repeated for ten times to obtain the CZTS precursor thin films. Finally, the CZTS precursor thin films and 1.1 g selenium powder were placed in a tube furnace. The CZTS precursor films were selenized at a high temperature at 550 °C for 30 min.

A X-ray diffractometer (XRD, D/MAX-Ultima IV, Rigaku) was first used to analyze the crystalline structure of the samples. A Raman spectrometer (OTBPI220-200-1, Zolix) with an excitation wavelength of 532 nm was used to further confirm the phase structure of samples. The surface and cross-sectional morphologies of the CZTSSe samples were characterized by scanning electron microscopy (SU8010, Hitachi). The current–voltage (*I–V*) curves of CZTSSe/Mo(S,Se)$_2$/Mo structure were obtained by *I–V* characteristic tester (SM-4, Semishare).

3. Results and discussion

Figure 1 shows the photos of the metal Mo foil substrate without pre-annealing and with different pre-annealing temperatures. The cleaned metal Mo foil substrate without pre-annealing appears silvery white. When the pre-annealing temperatures are 300 °C, 400 °C, and 500 °C, the surfaces of the Mo foil substrates are pale yellow, bluish violet, and gray, respectively. When the pre-annealed metal Mo foil substrates are immersed in concentrated ammonia solution, the surfaces of Mo foils are quickly dissolved within 1 min and become silver white. Therefore, it can be inferred that chemical reactions occur on the surfaces of Mo foils during pre-annealing treatment.

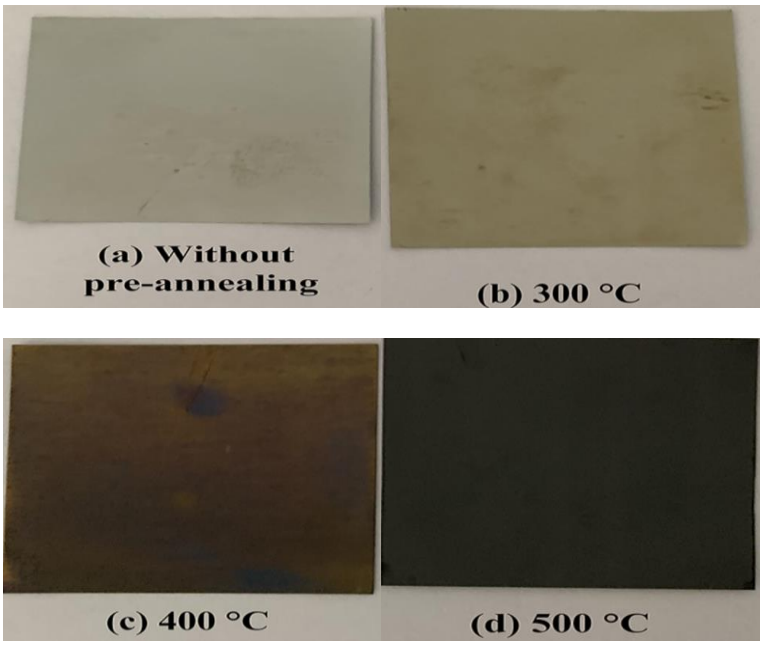

Fig. 1. The photos of Mo foil substrates (a) without pre-annealing and with pre-annealing temperature of (b) 300 °C, (c) 400 °C, and, (d) 500 °C.

Figure 2 shows the XRD patterns of the metal Mo foil substrates with and without pre-annealing. The substrate without pre-annealing has Mo diffraction peak at 59.1°, MoO_2 diffraction peak at 52.3°, and MoO_3 diffraction peak at 65.8°. After pre-annealing, more the diffraction peaks for MoO_3 and MoO_2 appear. When the pre-annealing temperature is 400 °C, the intensity of MoO_2 peak at 21.2° reaches the highest. When the pre-annealing temperature increases to 500 °C, the diffraction peaks of MoO_2 decrease and the MoO_3 peaks enhance. The XRD results show the oxidation of Mo foil after pre-annealing and the transformation from MoO_2 to MoO_3 with the increase of pre-annealing temperature.

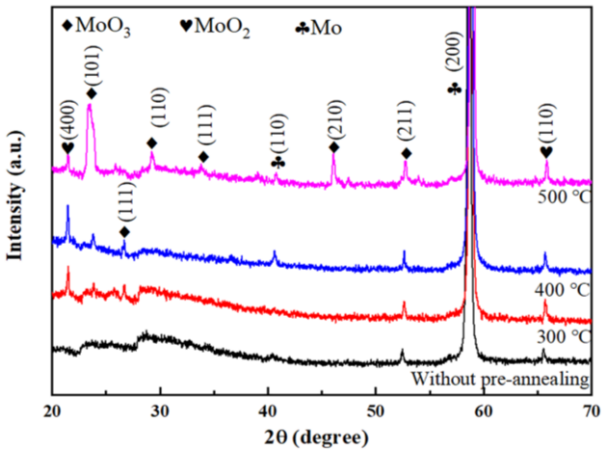

Fig. 2. The XRD patterns of Mo foil substrates without pre-annealing and with different pre-annealing temperatures.

Figure 3 shows the surface SEM images of Mo foil substrates without and with pre-annealing. The surface of Mo substrate without pre-annealing is relatively flat. When the pre-annealing temperature is 300 °C, grains are formed on the surface of the Mo substrate. With the increase of pre-annealing temperature, the grains enlarge from a few hundred nanometers to a few micrometers. According to the XRD and SEM results, it can be deduced that MoO_x is formed on the surface of metal Mo foil after pre-annealing.

Figure 4 shows the XRD patterns of the prepared CZTSSe samples on flexible Mo foil substrates. The crystalline diffraction peaks of all samples around 27.2°, 45.1°, and 53.5° are located between the standard diffraction peaks of $Cu_2ZnSnSe_4$ (CZTSe) and CZTS, indicating the incorporation of Se element into the CZTS precursor after selenization. $Mo(S,Se)_2$ diffraction peaks can be detected at 31.6° and 55.8°. The sample without pre-annealing has strong $Mo(S,Se)_2$ diffraction peaks. After pre-annealing treatment for the Mo foil substrate, the height of the $Mo(S,Se)_2$ diffraction peaks decrease with the increase of pre-annealing temperature. When the pre-annealing temperature reaches 500 °C, the $Mo(S,Se)_2$ peak at 55.8° disappears. These results indicate that the MoO_2 and MoO_3 on the surface of Mo foil can block the formation of $Mo(S,Se)_2$. Secondary phases of Cu_xSe_y and Sn_xS_y exist in all samples, and the intensity of peaks of secondary phases weakens as the pre-annealing temperature increases.

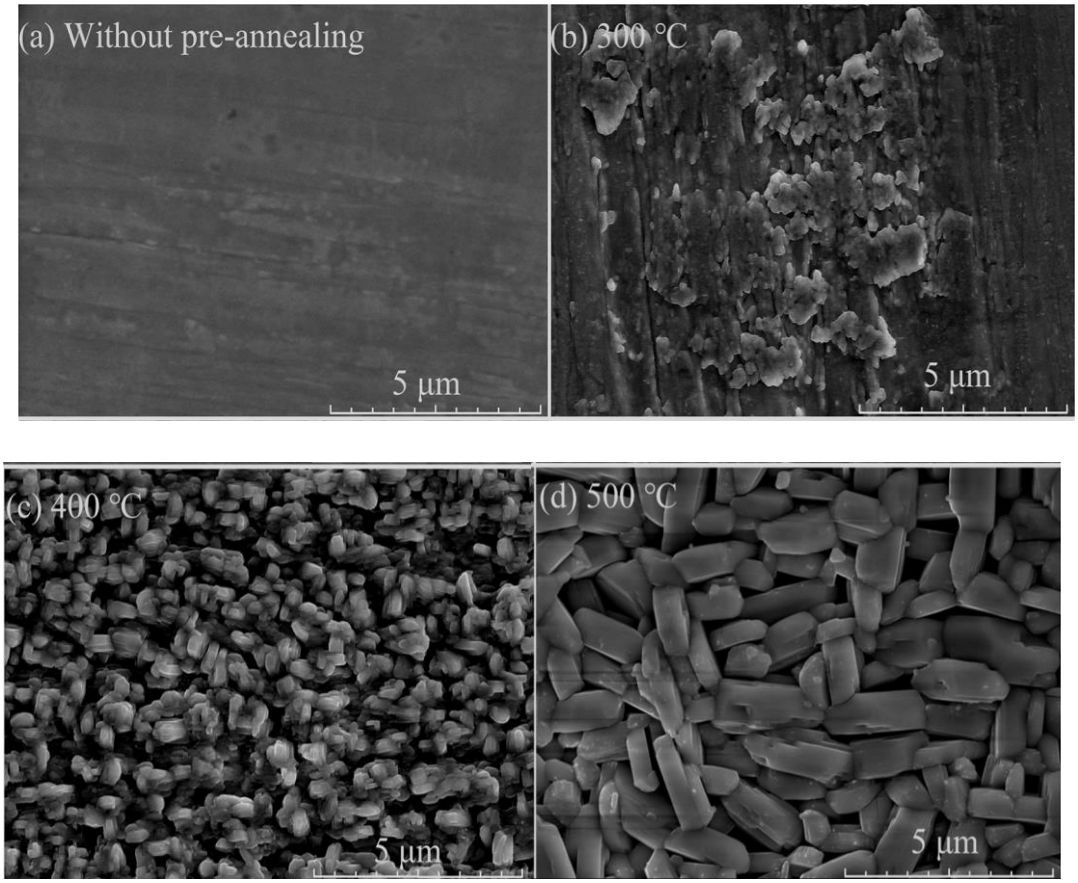

Fig. 3. The surface SEM images of Mo foil substrates (a) without pre-annealing and with pre-annealing temperatures of (b) 300 °C, (c) 400 °C, and (d) 500 °C.

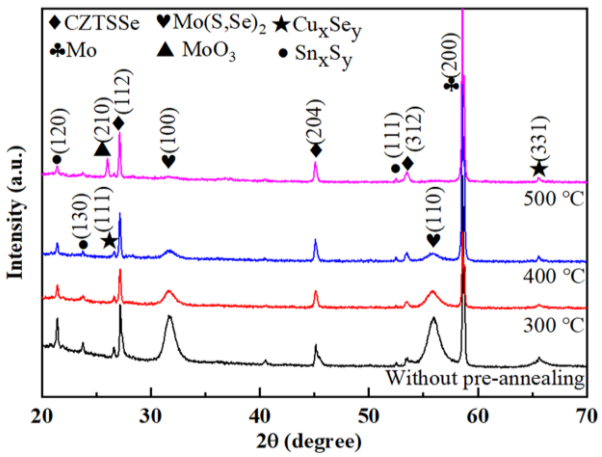

Fig. 4. The XRD patterns of CZTSSe thin films without substrate pre-annealing and with substrate pre-annealing at different temperatures.

Figure 5 shows the change in full width at half maximum (FWHM) of the (112) peak in XRD patterns and average size of periodic crystallites of CZTSSe with the change of pre-annealing temperatures of substrate. The average crystallite size (D) of CZTSSe on different substrates is estimated using Debye-Scherrer formula

$$D = \frac{K\lambda}{B\cos\theta} \tag{1}$$

where K is the Scherrer constant, B is the FWHM of the diffraction peak of the sample, θ is the Bragg angle, and λ is the X-ray wavelength. Compared with the sample without pre-annealing, the FWHM of (112) peak of the pre-annealed samples decreases and the average crystallite size increases. As the pre-annealing temperature increases, the FWHM of CZTSSe peak decreases, and the average crystallite size increases. The MoO_x(x=2,3) produced by the high-temperature pre-annealing is beneficial to the growth of CZTSSe grains because the MoO_x(x=2,3) blocks the reaction between Se vapor and Mo at the CZTSSe/Mo interface, which further makes Se vapor react with CZTS more fully.

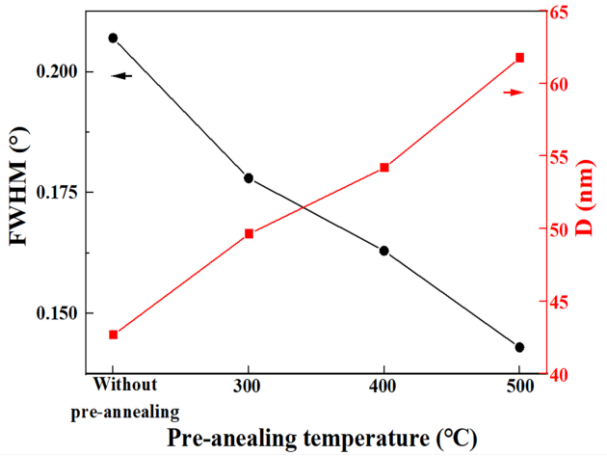

Fig. 5. The change of FWHM of the (112) peak in the XRD patterns and average crystallite size of CZTSSe with pre-annealing temperature.

The phase structures of prepared thin films were further measured by Raman spectroscopy, and the results are shown in Figure 6. The Raman peaks at around 190 cm^{-1} and 234 cm^{-1} are attributed to the vibration modes of CZTSSe. According to Ref. [24], for the sample without pre-annealing, the peak at 280 cm^{-1} originates from the vibration mode of Cu_xSe_y. After pre-annealing, the Cu_xSe_y peak cannot be detected. The $Mo(S,Se)_2$ peak is absent in all samples. The thickness of CZTSSe thin film of about 1 μm measured by cross-sectional SEM in the subsequent Figure 8 is larger than the detected depth of Raman measurement of 135 nm when the excitation wavelength is 532 nm. Therefore, Raman measurement cannot detect $Mo(S,Se)_2$ phase below the CZTSSe layer. Combining XRD patterns and Raman spectra, it is found that high-temperature pre-annealing of the metal Mo substrate inhibits the formation of $Mo(S,Se)_2$, Cu_xSe_y, and Sn_xS_y phases.

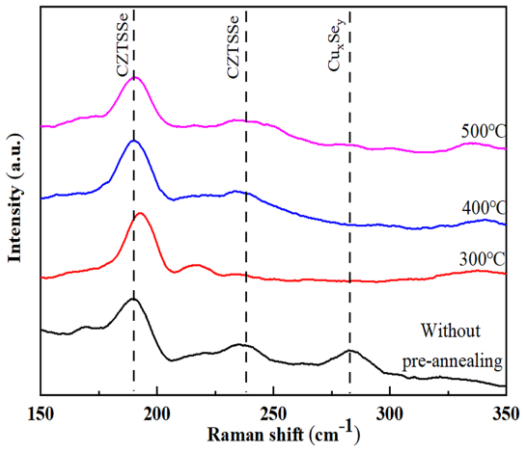

Fig. 6. Raman spectra of CZTSSe thin films without pre-annealing of substrate and with substrate annealing at different temperatures.

Figure 7 shows the surface SEM images of CZTSSe thin films. For the samples without pre-annealing, the surface of thin film is rough and uneven, and voids are formed. When the pre-annealing temperature of the Mo substrate increases from 300 °C to 500 °C, the surfaces of the CZTSSe thin films become flat and compact.

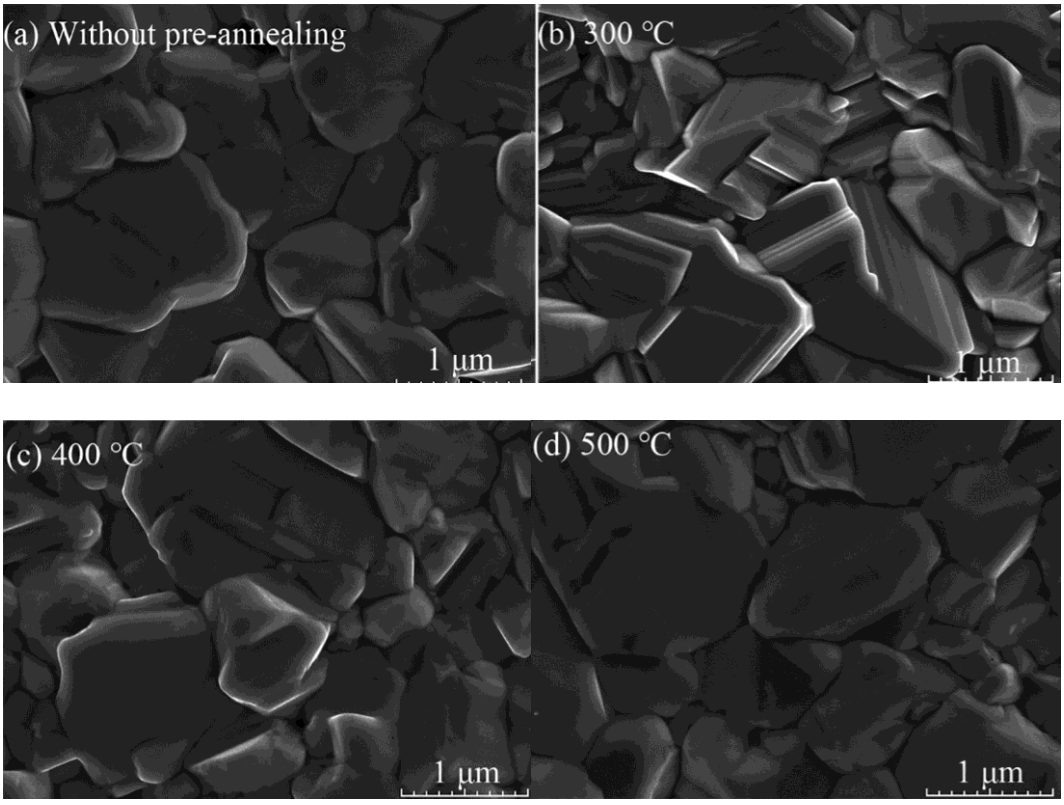

Fig. 7. The surface SEM images of CZTSSe thin films on Mo foil substrates (a) without pre-annealing and with pre-annealing temperature of (b) 300 °C, (c) 400 °C, and (d) 500 °C.

The cross-sectional SEM images of the CZTSSe samples without and with pre-annealing of Mo foil substrate are shown in Figure 8. For the sample without pre-annealing, there is a $Mo(S,Se)_2$ interface layer with a thickness of about 2.38 μm between the CZTSSe thin film and the Mo foil substrate. The thicknesses of the $Mo(S,Se)_2$ interface layer of samples with pre-annealing temperatures of 300 °C and 400 °C are about 2.15 μm and 1.65 μm, respectively. When the pre-annealing temperature is 500 °C, the thickness of $Mo(S,Se)_2$ reduces to about 0.85 μm.

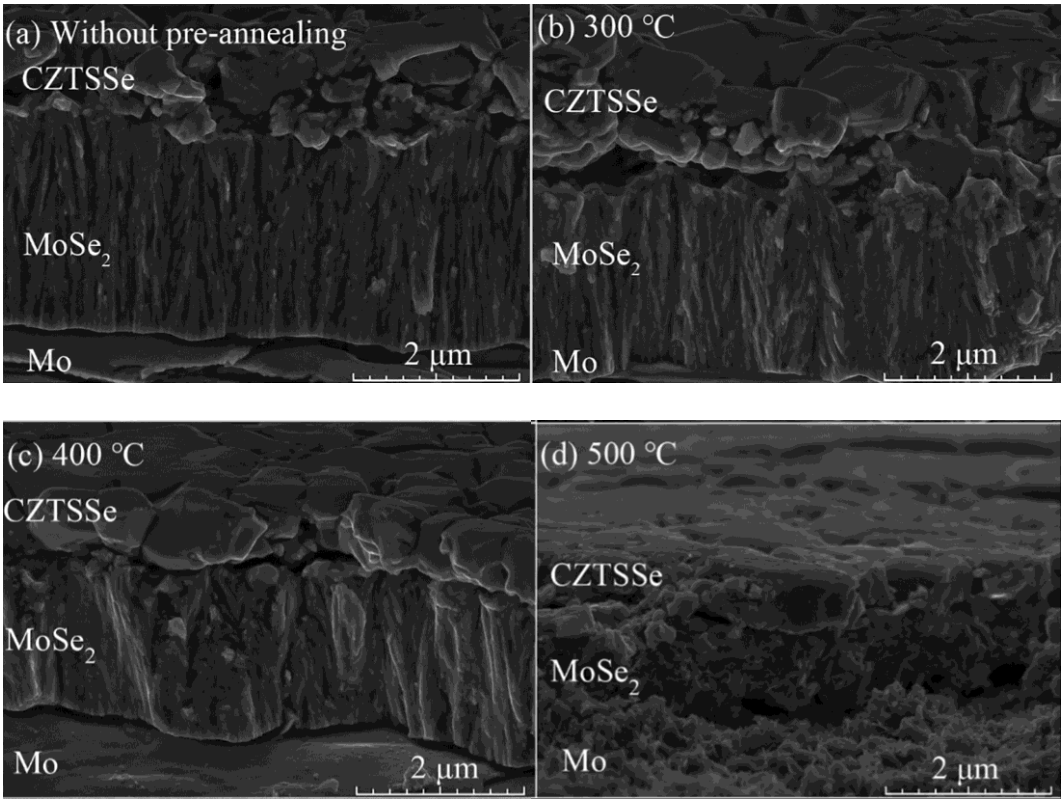

Fig. 8. The cross-sectional SEM images of CZTSSe thin films on Mo foil substrates (a) without pre-annealing and with pre-annealing temperature of (b) 300 °C, (c) 400 °C, and (d) 500 °C.

The *I–V* curves of the CZTSSe/$Mo(S,Se)_2$/Mo structure are shown in Figure 9. During the measurement of *I–V* curve, the sputtered Mo on the surface of CZTSSe was front electrode and the flexible Mo foil substrate was used as back electrode. The linear property of all *I–V* curves reveals the formation of ohmic contact between CZTSSe thin film and Mo foil substrate. Figure 10 shows the slope of *I–V* curve and resistance of the CZTSSe/$Mo(S,Se)_2$/Mo structure as a function of the substrate pre-annealing temperature. Substrate pre-annealing can increase the slope of the *I–V* curve of the CZTSSe/$Mo(S,Se)_2$/Mo structure and reduce the resistance of this structure. As the pre-annealing temperature of the Mo substrate increases, the thickness of the $Mo(S,Se)_2$ interface layer between the CZTSSe thin film and the Mo substrate decreases, which makes the resistance of the CZTSSe/$Mo(S,Se)_2$/Mo structure decreases. This indicates that pre-annealing of the metal substrate improves the ohmic contact characteristics between the CZTSSe thin film and the Mo foil substrate.

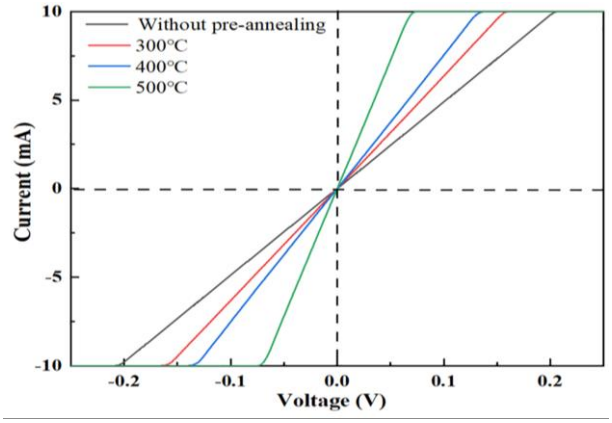

Fig. 9. The I–V curves of CZTSSe/Mo(S,Se)$_2$/Mo structure with different pre-annealing temperatures.

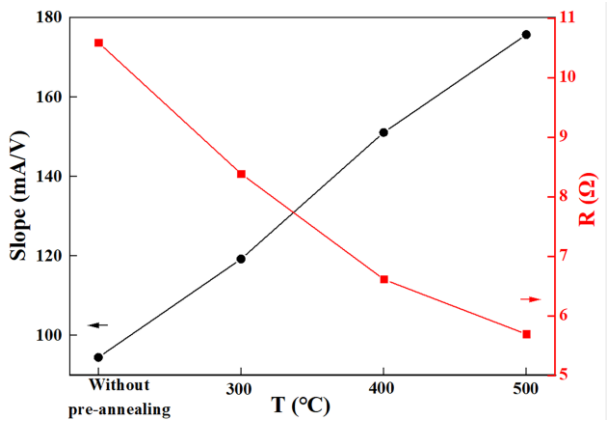

Fig. 10. The slope of I–V curves and the resistance of CZTSSe/Mo(S,Se)$_2$/Mo structure against the pre-annealing temperature.

4. Conclusion

This work focuses on the effect of substrate pre-annealing on the properties of CZTSSe thin film and CZTSSe/Mo interface. Flexible Mo foil substrates were first pre-annealed in air and then CZTSSe thin films were prepared on Mo foil substrates by sol-gel method. Compared with the sample without pre-annealing, the pre-annealing of Mo substrate can weaken the intensity of Mo(S,Se)$_2$ diffraction peak, increase the average crystallite size of CZTSSe to 62 nm, reduce the thickness of Mo(S,Se)$_2$ interface layer to 0.85 μm, increase the slope of the *I–V* curve of the CZTSSe/Mo(S,Se)$_2$/Mo structure to 0.18 S, and decrease the resistance of the CZTSSe/Mo(S,Se)$_2$/Mo structure to 5.7 Ω.

The inhibition of the formation of Mo(S,Se)$_2$ interface layer is ascribed to the formation of MoO_x on the surface of Mo foil substrate after pre-annealing. The MoO_x acts as a barrier to prevent the diffusion of Se into Mo foil substrate during the selenization process, which can suppress the formation of Mo(S,Se)$_2$ and reduce the thickness of Mo(S,Se)$_2$ interface layer. This work provides a facile method to adjust the back contact properties of CZTSSe thin film on flexible substrate.

References

[1] D.B. Mitzi, O. Gunawan, T.K. Todorov, K. Wang, S. Guha, Sol. Energy Mater. Sol. Cells 95, 1421 (2011); https://doi.org/10.1016/j.solmat.2010.11.028
[2] S.Y. Chen, A. Walsh, J.H. Yang, X.G. Gong, L. Sun, P.X. Yang, J.H. Chu, S.H. Wei, Phys. Rev. B 83, 113 (2011); https://doi.org/ 10.1103/PhysRevB.83.125201
[3] M. Grossberg, J. Krustok, J. Raudoja, K. Timmo, M. Altosaar, T. Raadik, Thin Solid Films 519, 7403 (2011); https://doi.org/10.1016/j.tsf.2010.12.099
[4] S. Giraldo, Z. Jehl, M. Placidi, V. Izquierdo-Roca, A. Perez-Rodriguez, E. Saucedo, Adv. Mater. 31, 1806692 (2019); https://doi.org/10.1002/adma.201806692
[5] W. Kogler, T. Schnabel, E. Ahlswede, M. Powalla, Sol. Energy Mater. Sol. Cells 200, 109959 (2019); https://doi.org/10.1016/j.solmat.2019.109959
[6] Sadanand, D.K. Dwivedi, Sol. Energy 193, 442 (2019); https://doi.org/10.1016/j.solener.2019.09.079
[7] J.Z. Zhou, X. Xu, B.W. Duan, H.J. Wu, J.J. Shi, Y.H. Luo, D.M. Li, Q.B. Meng, Nano Energy 89, 106405 (2021); https://doi.org/10.1016/j.nanoen.2021.106405
[8] M.P. Suryawanshi, G.L. Agawane, S.M. Bhosale, S.W. Shin, P.S. Patil, J.H. Kim, A.V. Moholkar, Mater. Thechnol. 28, 98 (2013); https://doi.org/10.1179/1753555712Y.0000000038
[9] G.A. Ren, D.M. Zhuang, M. Zhao, Y.W. Wei, Y.X. Wu, X.C. Li, X.Y. Lyu, C. Wang, Y.X. Li, Ceram. Int. 46, 13704 (2020); https://doi.org/10.1016/j.ceramint.2020.02.158
[10] H.Q. Xiao, W.H. Zhou, D.X. Kou, Z.J. Zhou, Y.N. Meng, Y.F. Qi, S.J. Yuan, L.T. Han, Z. Zheng, S.X. Wu, Sol. Energy Mater. Sol. Cells 231, 111308 (2021); https://doi.org/10.1016/j.solmat.2021.111308
[11] J. Zhao, X.H. Tan, W.N. Zhao, Y.K. Fang, X.X. Han, Appl. Phys. A. 127, 603 (2021); https://doi.org/10.1007/s00339-021-04753-w
[12] J. X. Xu, X. Tian, J. Ovonic. Res. 18, 227 (2022); https://doi.org/10.15251/JOR.2022.182.227
[13] T.J. Huang, X.S. Yin, G.J. Qi, H. Gong, Phys. Status Solidi-Rapid Res. Lett. 8, 735 (2015); https://doi.org/10.1002/pssr.201409219
[14] F.Y. Liu, S.X. Wu, Y. Zhang, X.J. Hao, L. Ding, Sci. Bull. 65, 698 (2020); https://doi.org/10.1016/j.scib.2020.02.014
[15] J.J. Scragg, J.T. Waetjen, M. Edoff, T. Ericson, T. Kubart, J. Am. Chem. Soc. 134, 19330 (2012); https://doi.org/10.1021/ja308862n
[16] V. Karade, A. Lokhande, P. Babar, M.G. Gang, M. Suryawanshi, P. Patil, J.H. Kim, Sol. Energy Mater. Sol. Cells. 200, 109911 (2019); https://doi.org/10.1016/j.solmat.2019.04.033
[17] Y.P. Song, B. Yao, Y.F. Li, Z.H. Ding, R.J. Liu, Y.R. Sui, L.G. Zhang, Z.Z. Zhang, H.F. Zhao, ACS Appl. Energ. Mater. 2, 2230 (2019); https://doi.org/10.1021/acsaem.8b02247
[18] X.H. Zhang, B. Yao, Y.F. Li, Z.H. Ding, H.F. Zhao, L.G. Zhang, Z.Z. Zhang, Sol. Energy 199, 128 (2020); https://doi.org/10.1016/j.solener.2020.02.033
[19] Y. Zeng, Z. Shen, X. Wu, D.X. Wang, Y.L. Wang, Y.L. Sun, L. Wu, Y. Zhang, J. Materiomics. 7, 470 (2021); https://doi.org/10.1016/j.jmat.2020.11.008
[20] X. Yu, S.Y. Cheng, Q. Yan, J.J. Fu, H.J. Jia, Q.Z. Sun, Z.Y. Yang, S.X. Wu, Sol. Energy Mater. Sol. Cells 209, 110434 (2020); https://doi.org/10.1016/j.solmat.2020.110434
[21] K.J. Yang, S. Kim, S.Y. Kim, K. Ahn, D.H. Son, S.H. Kim, S.J. Lee, Y.I. Kim, S.N. Park, S.J. Sung, D.H. Kim, T. Enkhbat, J. Kim, C.W. Jeon, J.K. Kang, Nat. Commun. 10, 2959 (2019);

https://doi.org/10.1038/s41467-019-10890-x
[22] B. Long, S.Y. Cheng, C. Yue, L.M. Dong, Micro Nano Lett. 13, 237 (2017);
https://doi.org/10.1049/mnl.2017.0471
[23] X.S. Wu, J.X. Xu, C.N. Zhuang, J. Mater. Sci. Mater. Electron. 32, 28373 (2021);
https://doi.org/10.1007/s10854-021-07217-2
[24] L. Korala, J.T. Mcgoffin, A.L. Prieto, ACS Appl. Mater. Interfaces 8, 4911 (2016);
https://doi.org/10.1021/acsami.5b11037